

Chia-Chang Liu
Graduate Student

Chung-Biau Tsay*
Professor,
ASME Mem.

Department of Mechanical Engineering
National Chiao Tung University
Hsinchu, Taiwan 300, R.O.C.

Tooth Undercutting of Beveloid Gears

A beveloid gear can be viewed as an involute gear of which the profile-shifted coefficient linearly decreases from the heel to the toe. Therefore, tooth undercutting occurs and singular points appear on the tooth surfaces near the toe. When undercutting occurs, the gear tooth is comparatively weak. In this study, the conditions of tooth undercutting of beveloid gears were derived and specific phenomena were also investigated by numerical illustrated examples. In addition, according to the characteristics of tooth undercutting on the beveloid gear tooth surface, two practicable methods were also proposed to avoid the tooth undercutting of beveloid gears. [DOI: 10.1115/1.1414128]

1 Introduction

Beveloid gears, also known as conical involute gears, can be viewed as involute gears with profile-shifted coefficient decreasing from the heel to the toe. Therefore, undercutting occurs and singular points appear on the negative profile-shifting tooth near the toe. Undercutting is an important aspect of gear design and manufacturing. It may cause weakness of gear strength, stress concentration and gear mismatch during gear meshing. When undercutting occurs, the strength of the gear is comparatively weak, resulting in a shortened service life of the gear set.

Beveloid gears have received considerable attention. In a pioneering work, Merritt [1] and Beam [2] proposed the basic characteristics and potentials of beveloid gears. Mitome [3–11] published the majority of the research on this subject. These investigations, however, focused largely on theoretical analyses, manufacture, measurements and bearing tests of beveloid gears. A complete mathematical model was not developed for beveloid gear tooth contact simulations. This study not only develops the mathematical model of beveloid gear according to the taper hobbing method [3,7] but also determines the conditions of tooth undercutting by adopting the method proposed by Litvin [12,13]. Meanwhile, specific phenomena of undercutting on the beveloid gear tooth are investigated by numerical illustrated examples. According to the results of undercutting analysis, two practicable methods that prevent the tooth undercutting of beveloid gears are also discussed in this study. One is the asymmetrical normal pressure angles for helical beveloid gear, and the other is the beveloid gear with varying working depth.

2 Mathematical Model of Beveloid Gears

2.1 Generation Concept. According to Merritt's generation concept [1], a beveloid gear can be generated by a basic rack whose pitch plane intersects with the axis of the gear and forms an angle equal to the generating cone angle. In practice, the most conventional method of beveloid gear manufacturing is the taper hobbing proposed by Mitome [3,7]. The imaginary rack cutter, which can be considered as the envelope generated by the hob in the space, is used to simulate the generating process of beveloid gears in this study.

2.2 Mathematical Model of Imaginary Rack Cutter. Figure 1 illustrates the normal section of the imaginary rack cutter. The two straight edges $M_0^{(l)}M_2^{(l)}$ and $M_0^{(r)}M_2^{(r)}$ can be represented in coordinate system $S_n(X_n, Y_n, Z_n)$ by

$$\begin{Bmatrix} x_n^{(i)} \\ y_n^{(i)} \\ z_n^{(i)} \end{Bmatrix} = \begin{Bmatrix} \ell^{(i)} \cos \alpha_n^{(i)} - a \\ \pm (\ell^{(i)} \sin \alpha_n^{(i)} - a \tan \alpha_n^{(i)} - b) \\ 0 \end{Bmatrix} \quad (i=l \text{ and } r), \quad (1)$$

where superscripts "l" and "r" denote the left and right side straight edges which generate the left and right side active tooth surfaces of the beveloid gear, respectively. The upper sign of Eq. (1) indicates the left side straight edge, while the lower sign represents the right side straight edge. According to Fig. 1, $\ell^{(i)} = |\overline{M_0^{(i)}M_1^{(i)}}|$ represents the design parameter; $\alpha_n^{(i)}$ denotes the normal pressure angle, and symbols P_n and p_n represent the gear diametral pitch and circular pitch, respectively.

Similarly, the left and right side fillets on the normal section of the imaginary rack cutter, which generate the fillet surfaces of the gear, can be expressed in coordinate system S_n as follows:

$$\begin{Bmatrix} x_n^{(i)} \\ y_n^{(i)} \\ z_n^{(i)} \end{Bmatrix} = \begin{Bmatrix} -\rho \cos \theta^{(i)} + \rho \sin \alpha_n^{(i)} - a \\ \pm (\rho \sin \theta^{(i)} - \rho \cos \alpha_n^{(i)} - a \tan \alpha_n^{(i)} - b) \\ 0 \end{Bmatrix} \quad (i=l \text{ and } r), \quad (2)$$

where $0 \leq \theta^{(i)} \leq (90 \text{ deg} - \alpha_n^{(i)})$ and $\theta^{(i)}$ represents the design parameter that determines the coordinates of any point on this fillet.

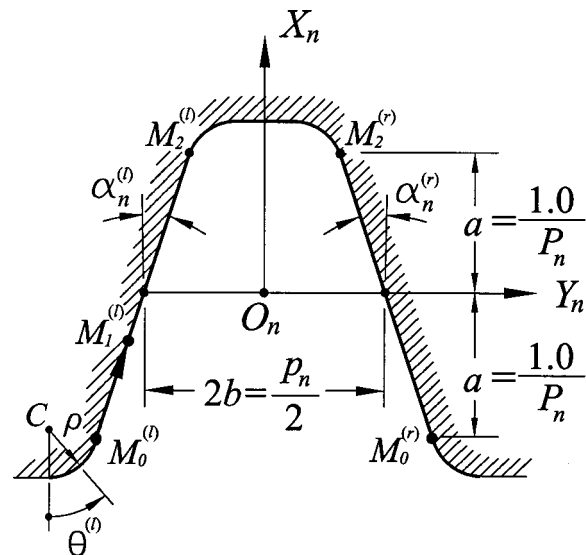


Fig. 1 The normal section imaginary rack cutter

*Corresponding author.

Contributed by the Power Transmission and Gearing Committee for publication in the JOURNAL OF MECHANICAL DESIGN. Manuscript received May 2000. Associate Editor: R. F. Handschuh.

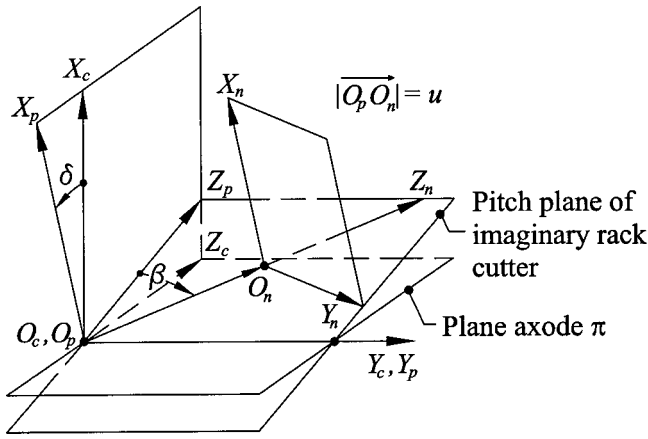


Fig. 2 Relations among coordinate systems S_n , S_p and S_c

To obtain the imaginary rack cutter surface, the normal section of the imaginary rack cutter is attached to the plane $X_n - Y_n$ and translated along the line $\overline{O_p O_n}$ with respect to the coordinate system $S_p(X_p, Y_p, Z_p)$, as illustrated in Fig. 2. Herein, $u = |\overline{O_p O_n}|$ is a design parameter of the imaginary rack cutter surface. The profile of the imaginary rack cutter can thus be traced out in coordinate system S_p , and the plane $Y_p - Z_p$ can be regarded as the pitch plane of the imaginary rack cutter. The angle β , which determines the direction of tooth trace, is the helix angle on the pitch plane of imaginary rack cutter. In order to simulate the taper hobbing process, the coordinate system S_p is then set to form an inclined angle δ with respect to the plane axode coordinate system $S_c(X_c, Y_c, Z_c)$. The straight-edge surfaces of the imaginary rack cutter surface can thus be represented in coordinate system S_c as follows:

$$\begin{aligned} x_c^{(i)} &= (\ell^{(i)} \cos \alpha_n^{(i)} - a) \cos \delta + [\mp (\ell^{(i)} \sin \alpha_n^{(i)} \\ &\quad - a \tan \alpha_n^{(i)} - b) \sin \beta + u \cos \beta] \sin \delta, \\ y_c^{(i)} &= \pm (\ell^{(i)} \sin \alpha_n^{(i)} - a \tan \alpha_n^{(i)} - b) \cos \beta + u \sin \beta, \end{aligned}$$

and

$$\begin{aligned} z_c^{(i)} &= -(\ell^{(i)} \cos \alpha_n^{(i)} - a) \sin \delta + [\mp (\ell^{(i)} \sin \alpha_n^{(i)} \\ &\quad - a \tan \alpha_n^{(i)} - b) \sin \beta + u \cos \beta] \cos \delta, \end{aligned} \quad (3)$$

where $i=l$ and r .

Meanwhile, the fillet surfaces of the imaginary rack cutter can be represented in coordinate system S_c as follows:

$$\begin{aligned} x_c^{(i)} &= (-\rho \cos \theta^{(i)} + \rho \sin \alpha_n^{(i)} - a) \cos \delta + [\mp (\rho \sin \theta^{(i)} \\ &\quad - \rho \cos \alpha_n^{(i)} - a \tan \alpha_n^{(i)} - b) \sin \beta + u \cos \beta] \sin \delta, \\ y_c^{(i)} &= \pm (\rho \sin \theta^{(i)} - \rho \cos \alpha_n^{(i)} - a \tan \alpha_n^{(i)} - b) \cos \beta + u \sin \beta, \end{aligned}$$

and

$$\begin{aligned} z_c^{(i)} &= -(-\rho \cos \theta^{(i)} + \rho \sin \alpha_n^{(i)} - a) \sin \delta + [\mp (\rho \sin \theta^{(i)} \\ &\quad - \rho \cos \alpha_n^{(i)} - a \tan \alpha_n^{(i)} - b) \sin \beta + u \cos \beta] \cos \delta, \end{aligned} \quad (4)$$

where $i=l$ and r .

Since the surface coordinates of imaginary rack cutter are ℓ and u for the straight-edge surfaces and θ and u for the fillet surfaces, the unit normal to the rack cutter surface can be represented by the subsequent equations:

$$n_c = \frac{N_c}{|N_c|}, \quad (5)$$

where

$$N_c = \frac{\partial R_c}{\partial u} \times \frac{\partial R_c}{\partial \ell} \quad (\text{for the straight-edge surfaces}),$$

and

$$N_c = \frac{\partial R_c}{\partial u} \times \frac{\partial R_c}{\partial \theta} \quad (\text{for the fillet surfaces}).$$

Equations (3) and (5) result in the unit normal to the straight-edge surfaces of imaginary rack cutter as follows:

$$\begin{aligned} n_{xc}^{(i)} &= -\cos \alpha_n^{(i)} \sin \beta \sin \delta \mp \sin \alpha_n^{(i)} \cos \delta, \\ n_{yc}^{(i)} &= \cos \alpha_n^{(i)} \cos \beta, \end{aligned}$$

and

$$n_{zc}^{(i)} = -\cos \alpha_n^{(i)} \sin \beta \cos \delta \pm \sin \alpha_n^{(i)} \sin \delta \quad (i=l \text{ and } r). \quad (6)$$

Equations (4) and (5) result in the unit normal to the fillet surfaces of imaginary rack cutter as follows:

$$\begin{aligned} n_{xc}^{(i)} &= -\sin \beta \sin \delta \sin \theta^{(i)} \mp \cos \delta \cos \theta^{(i)}, \\ n_{yc}^{(i)} &= \cos \beta \sin \theta^{(i)}, \end{aligned}$$

and

$$n_{zc}^{(i)} = -\sin \beta \cos \delta \sin \theta^{(i)} + \sin \delta \cos \theta^{(i)} \quad (i=l \text{ and } r). \quad (7)$$

2.3 Mathematical Model of Beveloid Gear Tooth Surface.

Figure 3 schematically depicts the gear generation mechanism and the coordinate relationship between the plane axode π and the gear axode. Herein, r_1 and P_0 denote the pitch radius and pitch point of the generated beveloid gear, and ϕ_1 represents the gear rotation angle in the generating process. The coordinate system $S_f(X_f, Y_f, Z_f)$ represents the fixed coordinate system, while $S_1(X_1, Y_1, Z_1)$ is the coordinate system attached to the generated gear, and S_c is the plane axode coordinate system attached to the imaginary rack cutter. Based on the theory of gearing [12,13], the mathematical model of the generated tooth surface can be attained by simultaneously considering the equation of meshing together with the locus of the imaginary rack cutter represented in gear coordinate system S_1 . The mathematical model of the beveloid gear can be obtained and represented in coordinate system S_1 as follows:

$$R_1 = [M_{1c}] R_c, \quad (8)$$

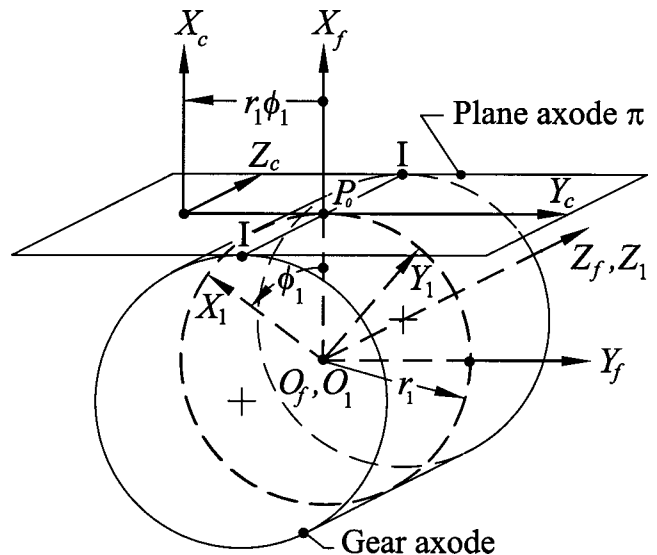


Fig. 3 Coordinate relationship between the imaginary rack and cutter generated gear

and

$$\frac{X_c - x_c}{n_{xc}} = \frac{Y_c - y_c}{n_{yc}} = \frac{Z_c - z_c}{n_{zc}}. \quad (9)$$

Equation (8) is the locus of rack cutter surface R_c represented in coordinate system S_1 , and Eq. (9) represents the equation of meshing. Herein, X_c , Y_c and Z_c are the coordinates of a point on the instantaneous axis of gear rotation I-I, which is represented in coordinate system S_c ; n_{xc} , n_{yc} and n_{zc} are the directional components of the surface unit normal n_c . Equations (6)–(9) yield the generated tooth surface in coordinate system S_1 as follows:

$$\begin{cases} x_1 \\ y_1 \\ z_1 \end{cases} = \begin{cases} x_c \cos \phi_1 - y_c \sin \phi_1 + r_1 (\cos \phi_1 + \phi_1 \sin \phi_1) \\ x_c \sin \phi_1 + y_c \cos \phi_1 + r_1 (\sin \phi_1 - \phi_1 \cos \phi_1) \\ z_c \end{cases}, \quad (10)$$

where

$$\phi_1 = (y_c n_{xc} - x_c n_{yc}) / (r_1 n_{xc}). \quad (11)$$

Herein, Eq. (11) comes from Eq. (9). Substituting Eqs. (3) and (6) and Eqs. (4) and (7) into Eqs. (10) and (11) allow us to obtain the mathematical model of the beveloid gear represented in coordinate system S_1 .

3 Undercutting Analysis

Mathematically, the phenomenon of tooth undercutting is the appearance of singular points on the active tooth surface. To compute the singular points on the active tooth surface and determine their corresponding parameters on the straight-edge surface of imaginary rack cutter, this work adopts the method proposed by Litvin [12,13] which considered the relative velocity and equation of meshing between the imaginary rack cutter and generated gear.

3.1 Calculation of Relative Velocity. According to the generation mechanism mentioned above, the absolute velocities of the imaginary rack cutter and generated gear can be decomposed into two components: transfer velocity V_{tr} and relative velocity V_r . Due to the continuity of contact between the cutter and generated tooth surface, the absolute velocities of the imaginary rack cutter and generated gear are the same at the point of contact and can be related as

$$V^{(abs)} = V_{tr}^{(c)} + V_r^{(c)} = V_{tr}^{(1)} + V_r^{(1)}, \quad (12)$$

or

$$V_r^{(1)} = V_r^{(c)} + (V_{tr}^{(c)} - V_{tr}^{(1)}) = V_r^{(c)} + V^{(c1)}, \quad (13)$$

where subscript “r” represents the relative motion over the cutter surface and subscript “tr” represents the transfer motion with the imaginary rack cutter and generated gear. Superscript “c” represents the cutter and superscript “1” represents the generated gear. According to Fig. 3, the relative velocity between the imaginary rack cutter and generated gear can be represented in S_c coordinate system as follows:

$$V_c^{(c1)} = V_c^{(c)} - V_c^{(1)}, \quad (14)$$

where

$$\begin{aligned} V_c^{(1)} &= \omega_1 \times R_c + \overline{O_c O_1} \times \omega_1 \\ &= [\omega_1 (y_c - r_1 \phi_1)] \mathbf{i}_c + [\omega_1 (-x_c - r_1)] \mathbf{j}_c, \end{aligned} \quad (15)$$

and

$$V_c^{(c)} = -\omega_1 r_1 \mathbf{j}_c. \quad (16)$$

Herein, ω_1 is the angular velocity of the generated gear and can be obtained by $d\phi_1/dt$.

3.2 Conditions of Undercutting. The surface tangent T exists at any regular point on the active tooth surface, i.e., $T \neq 0$.

Based on differential geometry, the tangent vector T to the generated surface is collinear with its relative velocity $V_r^{(1)}$. When undercutting occurs, a singular point appears on the active tooth surface and the tangent vector becomes $T=0$ at this singular point. Restated, the relative velocity at a singular point on the active tooth surface equals zero, that is

$$V_r^{(1)} = V_r^{(c)} + V^{(c1)} = 0 \quad (17)$$

Since the surface coordinates of imaginary rack cutter are ℓ and u for the straight-edge surface that generates the active tooth surface of beveloid gears, Eq. (17) can be decomposed into three components along X_c -axis, Y_c -axis and Z_c -axis as follows:

$$\frac{\partial x_c}{\partial \ell} \frac{d\ell}{dt} + \frac{\partial x_c}{\partial u} \frac{du}{dt} = -V_{xc}^{(c1)}, \quad (18)$$

$$\frac{\partial y_c}{\partial \ell} \frac{d\ell}{dt} + \frac{\partial y_c}{\partial u} \frac{du}{dt} = -V_{yc}^{(c1)}, \quad (19)$$

and

$$\frac{\partial z_c}{\partial \ell} \frac{d\ell}{dt} + \frac{\partial z_c}{\partial u} \frac{du}{dt} = -V_{zc}^{(c1)}. \quad (20)$$

Recalling that either Eq. (9) or Eq. (11) represent the equation of meshing between the generated tooth surface and the imaginary rack cutter. It is rewritten here for convenience:

$$f(\phi_1, \ell, u) = (r_1 \phi_1 - y_c) n_{xc} + x_c n_{yc} = 0 \quad (21)$$

Differentiation of the equation of meshing, i.e., Eq. (21), yields

$$\frac{\partial f}{\partial \ell} \frac{d\ell}{dt} + \frac{\partial f}{\partial u} \frac{du}{dt} = -\frac{\partial f}{\partial \phi_1} \frac{d\phi_1}{dt}. \quad (22)$$

Equations (18), (19), (20), and (22) form a system of four linear equations with two unknown $d\ell/dt$ and du/dt which provide a method for determining the conditions of gear undercutting. The system of equations possesses a unique solution if the rank of the matrix

$$A = \begin{bmatrix} \frac{\partial R_c}{\partial \ell} & \frac{\partial R_c}{\partial u} & -V_c^{(c1)} \\ \frac{\partial f}{\partial \ell} & \frac{\partial f}{\partial u} & -\frac{\partial f}{\partial \phi_1} \frac{d\phi_1}{dt} \end{bmatrix} \quad (23)$$

is equal to two. This yields the following three equality equations:

$$\Delta_1 = \begin{vmatrix} \frac{dx_c}{d\ell} & \frac{dx_c}{du} & -V_{xc}^{(c1)} \\ \frac{dy_c}{d\ell} & \frac{dy_c}{du} & -V_{yc}^{(c1)} \\ \frac{\partial f}{\partial \ell} & \frac{\partial f}{\partial u} & -\frac{\partial f}{\partial \phi_1} \frac{d\phi_1}{dt} \end{vmatrix} = 0, \quad (24)$$

$$\Delta_2 = \begin{vmatrix} \frac{dx_c}{d\ell} & \frac{dx_c}{du} & -V_{xc}^{(c1)} \\ \frac{dz_c}{d\ell} & \frac{dz_c}{du} & -V_{zc}^{(c1)} \\ \frac{\partial f}{\partial \ell} & \frac{\partial f}{\partial u} & -\frac{\partial f}{\partial \phi_1} \frac{d\phi_1}{dt} \end{vmatrix} = 0, \quad (25)$$

and

Table 1 Some major design parameters of beveloid gears

Normal module	$m_n = 5 \text{ (mm / teeth)}$
Fillet radius	$\rho = 0.3 \text{ mm}$
Normal pressure angle	$\alpha_n^{(l)} = \alpha_n^{(r)} = 20^\circ$
Cone angle	$\delta = 20^\circ$
Number of teeth	$N_1 = 25$
Face width (Thickness of gear blank)	$F = 20 \text{ (mm)}$

$$\Delta_3 = \begin{vmatrix} \frac{dy_c}{d\ell} & \frac{dy_c}{du} & -V_{yc}^{(c1)} \\ \frac{dz_c}{d\ell} & \frac{dz_c}{du} & -V_{zc}^{(c1)} \\ \frac{\partial f}{\partial \ell} & \frac{\partial f}{\partial u} & -\frac{\partial f}{\partial \phi_1} \frac{d\phi_1}{dt} \end{vmatrix} = 0. \quad (26)$$

Equation (24)–(26) can be applied to determine the conditions of singularity, and the sufficient condition for singularity can be represented by

$$\Delta_1^2 + \Delta_2^2 + \Delta_3^2 = F(\ell, u, \phi_1) = 0 \quad (27)$$

Thus, the undercutting condition on the active tooth surface of the proposed beveloid gear can be calculated by applying the numerical method with Eq. (27). By applying the method mentioned above, undercutting conditions can be calculated and undercutting lines can be plotted on the beveloid gear tooth surfaces by applying the computer graphical method. Illustrative examples are presented to demonstrate the effectiveness of the proposed mathematical model and undercutting analysis.

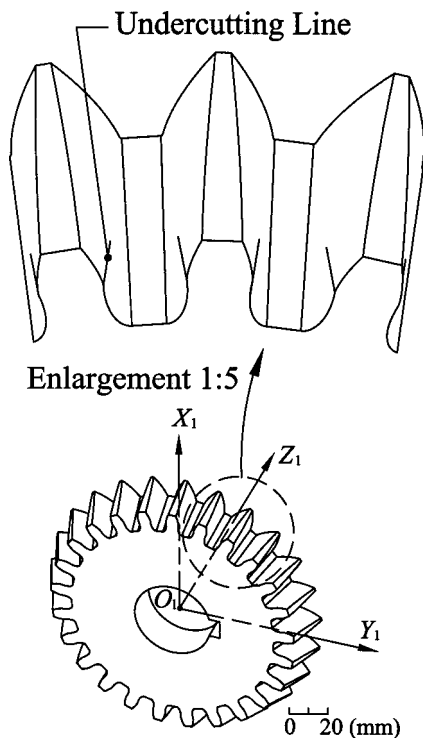


Fig. 4 Undercutting of straight beveloid gear

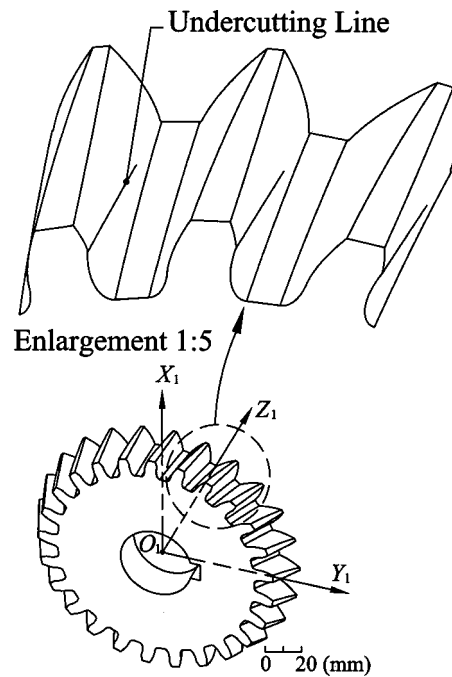


Fig. 5 Undercutting of helical beveloid gear

Example 1: Tooth Undercutting of Straight Beveloid Gears.

Table 1 summarizes some major design parameters of the straight beveloid gear with $\beta = 0$ deg. Figure 4 shows the undercutting lines that were numerically solved by the developed computer programs. Notably, a beveloid gear can be viewed as an involute gear of which the profile-shifted coefficient linearly decreases from heel to toe. Therefore, the tooth undercutting lines appear near the toe of the beveloid gear tooth surface where negative profile-shifting becomes severe. Owing to the symmetry of straight beveloid gear teeth, the undercutting is symmetrical on both sides of the tooth surfaces.

Example 2: Tooth Undercutting of Helical Beveloid Gears.

Figure 5 illustrates the tooth undercutting of a helical beveloid gear. The major design parameters are chosen the same as those listed in Table 1. The helix angle on the pitch plane of the imaginary rack cutter is $\beta = 15$ deg (right handed). As illustrated in Fig. 5, the undercutting lines appear only on the right side of the tooth surfaces. This phenomenon is due to the fact that the gear has different pressure angles for the left and right side tooth surfaces on the plane of rotation. The detail will be discussed in the next section.

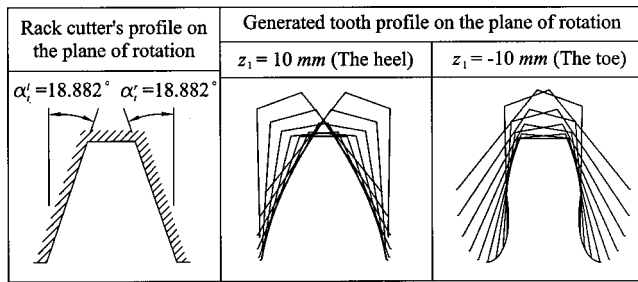
4 Tooth Profile Analysis on the Plane of Rotation

In 1983, Mitome proposed the parametric design of the beveloid gear. That investigation also proposed the tooth undercutting condition of beveloid gears by the limitation of the base circle. To verify the accuracy of the proposed mathematical model and undercutting analysis, the tooth profile on the plane of rotation is discussed hereinafter. Theoretically, a beveloid gear can be represented as an infinite succession of two-dimensional involute gears with profile-shifted coefficient linearly decreasing from heel to toe. To express the profile of the imaginary rack cutter on the plane of rotation (i.e. $X_c - Y_c$ plane), the third item of Eq. (3) can be adapted as follows:

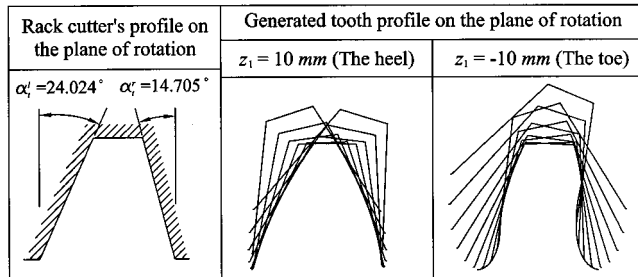
$$u = [z_c^{(i)} + (\ell^{(i)} \cos \alpha_n^{(i)} - a) \sin \delta \pm (\ell^{(i)} \sin \alpha_n^{(i)} - a \tan \alpha_n^{(i)} - b) \times \sin \beta \cos \delta] / (\cos \beta \cos \delta), \quad (28)$$

where $i = l$ and r .

Similarly, the third item of Eq. (4) can be adapted as follows:



(a)



(b)

Fig. 6 The profiles of rack cutter and generated beveloid gear on the plane rotation; (a) straight beveloid gear, (b) helical beveloid gear

$$u = [z_c^{(i)} + (-\rho \cos \theta^{(i)} + \rho \sin \alpha_n^{(i)} - a) \sin \delta \pm (\rho \sin \theta^{(i)} - \rho \cos \alpha_n^{(i)} - a \tan \alpha_n^{(i)} - b) \sin \beta \cos \delta] / (\cos \beta \cos \delta), \quad (29)$$

where $i=l$ and r .

Considering the first two items of Eq. (3) together with Eq. (28) and the first two items of Eq. (4) together with Eq. (29), the profile of the two-dimensional imaginary rack cutter can be obtained and expressed on the plane of rotation by treating z_c as a constant. By taking the arctangent to the slope of the straight edges of the two-dimensional imaginary rack cutter, the pressure angles on the plane of rotation can be obtained and expressed by:

$$\alpha_t^{(i)} = \tan^{-1} \left(\frac{\pm \cos \alpha_n^{(i)} \sin \beta \sin \delta + \sin \alpha_n^{(i)} \cos \delta}{\cos \alpha_n^{(i)} \cos \beta} \right), \quad (30)$$

where $i=l$ and r . Substituting the profile of the two-dimensional imaginary rack cutter into Eqs. (10) and (11) results in the profile of the beveloid gear on the plane of rotation. According to the fundamentals of an involute gear, the base radius of the beveloid gear can be expressed as:

$$r_b^{(i)} = r_1 \cos \alpha_t^{(i)}, \quad (31)$$

where $i=l$ and r . Therefore, the straight beveloid gear discussed in Example 1 and helical beveloid gear obtained in Example 2 can be analyzed and illustrated on the plane of rotation. By applying Eq. (30), the left and right side pressure angles of the straight beveloid gear on the plane of rotation are $\alpha_t^{(l)} = \alpha_t^{(r)} = 18.882^\circ$, as shown in Fig. 6(a). Thus, the profile of straight beveloid gear tooth on the plane of rotation is symmetrical, and the base radius can be calculated as $r_b^{(l)} = r_b^{(r)} = 59.1368 \text{ mm}$. The coordinates of some undercutting points on both sides of the tooth surfaces are calculated and listed in Table 2. By calculating the distances from the gear axis (i.e. Z_1 -axis) to these undercutting points, all undercutting points are found located on the base cylinder with $r_b^{(l)} = r_b^{(r)} = 59.1368 \text{ mm}$. This result satisfies the fundamentals of an involute gear and also verifies the accuracy of the proposed undercutting analysis. Observing the tooth profiles on the planes of rotation with $Z_1 = 10 \text{ mm}$ and $Z_1 = -10 \text{ mm}$, as

Table 2 Undercutting points of straight beveloid gears (left and right side tooth surfaces) unit : mm

X_1	Y_1	Z_1	$\sqrt{X_1^2 + Y_1^2}$
58.9985	± 4.0413	-3.4706	59.1368
59.0111	± 3.8537	-5.0669	59.1368
59.0230	± 3.6660	-6.6632	59.1368
59.0344	± 3.4784	-8.2594	59.1368
59.0452	± 3.2907	-9.8557	59.1368

shown in Fig. 6(a), the long addendum tooth with a positive profile-shifted coefficient and the short addendum tooth with a negative profile-shifted coefficient may appear near the heel and the toe, respectively. The demonstration of the loci of the imaginary rack cutter and the generated tooth profile on the plane of rotation avail the understanding of undercutting phenomenon near the toe.

Figure 6(b) illustrates the plane of rotation of the helical beveloid gear as discussed in Example 2. According to our results, the left and right side pressure angles of the helical beveloid gear on the plane of rotation are $\alpha_t^{(l)} = 24.024^\circ$ and $\alpha_t^{(r)} = 14.705^\circ$. Therefore, the tooth profile is no longer symmetrical on the plane of rotation, and the base radius of the left and right side tooth surfaces of this helical beveloid gear can be calculated as $r_b^{(l)} = 59.0997 \text{ mm}$ and $r_b^{(r)} = 62.5854 \text{ mm}$, respectively. The coordinates of some undercutting points on the right side tooth surface are calculated and listed in Table 3(a). By calculating the distances from the gear axis to these undercutting points, we can find that all undercutting points are located on the base cylinder with $r_b^{(r)} = 62.5854 \text{ mm}$. The coordinates of undercutting points on the left side tooth surface are also listed in Table 3(b). Although all undercutting points are located on the base cylinder with $r_b^{(l)} = 59.0997 \text{ mm}$, they only exist in the region of $z_1 \leq -15.0801 \text{ mm}$, which is out of the range of the face width (i.e. $-10 \text{ mm} \leq x_1 \leq 10 \text{ mm}$) of the beveloid gear we discussed herein. A comparison of the left and right side tooth surfaces on the plane of rotation reveals that tooth undercutting occurs only on the right

Table 3 Undercutting points of helical beveloid gear

(a) right side tooth surface unit : mm

X_1	Y_1	Z_1	$\sqrt{X_1^2 + Y_1^2}$
62.3519	5.4010	3.0233	62.5854
62.4553	4.0327	-0.7037	62.5854
62.5121	3.0280	-3.4367	62.5854
62.5609	1.7482	-6.9152	62.5854
62.5820	0.6506	-9.8967	62.5854

(b) left side tooth surface unit : mm

X_1	Y_1	Z_1	$\sqrt{X_1^2 + Y_1^2}$
58.6894	-6.9524	-15.0801	59.0997
58.6752	-7.0710	-16.1445	59.0997
58.6608	-7.1896	-17.2089	59.0997
58.6461	-7.3082	-18.2733	59.0997
58.6275	-7.4564	-19.6039	59.0997

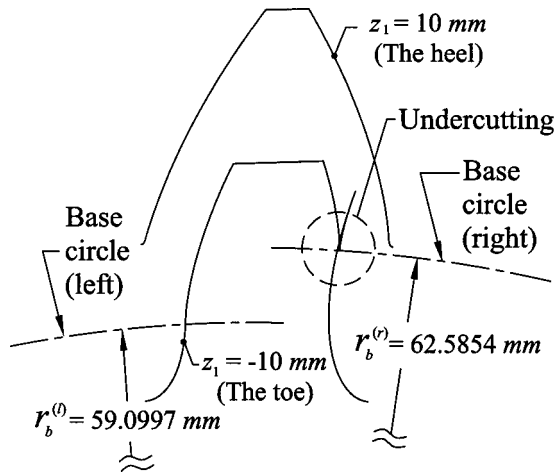


Fig. 7 The tooth profile of helical beveloid gear ($\alpha_n^{(l)} = \alpha_n^{(r)} = 20$ deg) and base circles on the plane of rotation

side tooth surface, which has a larger base radius caused by a smaller pressure angle. Figure 7 presents the helical beveloid gear tooth on the plane of rotation together with the base circles of the left and right side tooth surfaces, respectively. On the plane of rotation near the toe ($Z_1 = -10$ mm), the right side active tooth touches the base circle (i.e. radius $r_b^{(r)}$) and has a singular point on it. However, the left side active tooth surface is located above the base circle (i.e. radius $r_b^{(l)}$), and no singular point exists. Meanwhile, since the tooth has a positive profile-shifted coefficient on the plane of rotation near the heel ($Z_1 = 10$ mm), the entire active tooth profile is located above the base circles of radii $r_b^{(l)}$ and $r_b^{(r)}$, thus, no undercutting occurs on either side of the tooth surface. Figure 8 illustrates the enlargement of tooth undercutting as demonstrated in Fig. 7. Notably, the undercutting point acquired by solving the singularity may be treated as the “theoretical undercutting point.” After the generating process, part of the active tooth may be cut by the generation line of the fillet region and the “theoretical undercutting point” is no longer existent. As shown in Fig. 8, the “actual undercutting point,” which can be solved by a numerical method, is the intersecting point of the generation lines of active tooth and fillet.

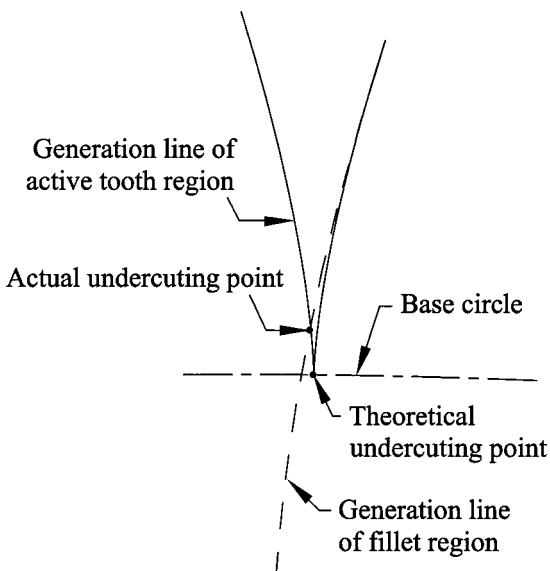


Fig. 8 The theoretical and actual tooth undercutting points

5 Undercutting Prevention

Referring to the fundamentals of an involute gear, some principals, such as positive profile shifting, a higher pressure angle, a larger number of gear teeth, the adoption of stub teeth, etc., were suggested to prevent tooth undercutting. In this section, two practicable methods are proposed to prevent tooth undercutting of beveloid gears.

5.1 Helical Beveloid Gear with Asymmetrical Normal Pressure Angles. According to the tooth profile of helical beveloid gear on the plane of rotation shown in Fig. 6(b) and Fig. 7, tooth undercutting occurs only on the right side tooth surface, which has a larger base radius caused by a smaller pressure angle. By selecting a larger normal pressure angle for the right side of the imaginary rack cutter (Fig. 1), e.g., $\alpha_n^{(r)} = 30$ deg, the right side pressure angle on the plane of rotation thus becomes $\alpha_t^{(r)} = 25.175$ deg. As illustrated in Fig. 9, the base radius of the right side tooth surface reduces to $r_b^{(r)} = 58.5588$ mm, which makes the whole right side active tooth surface located above the base circle, and no singular point exists. Therefore, this helical beveloid gear with asymmetrical normal pressure angles (i.e. $\alpha_n^{(l)} = 20$ deg and $\alpha_n^{(r)} = 30$ deg) not only prevent the tooth undercutting on the right side tooth surface, but also remain the advantage of small pressure angle, such as higher contact ratio and lower radial thrust, etc., for the left side tooth surface.

5.2 Beveloid Gear with Varying Working Depth. As mentioned above, the undercutting condition of a beveloid gear can be considered as the limitation of the base circle. Therefore, Mitome [10] proposed the straight beveloid gear with stub teeth to avoid undercutting by reducing the cutting depth. Applying the proposed mathematical model, the beveloid gear with stub teeth can be acquired by choosing the parameter $a < 1.0/P_n$ (refer to Fig. 1). Though stub teeth prevent undercutting on the toe region, the active tooth profile in the central region of the tooth width where bearing contact located is also shortened. Thus, the contact ratio may decrease. In order to prevent tooth undercutting on the toe and to maintain a full working tooth on the central region of the tooth width, a new generating concept and a practicable hobbing method of novel type beveloid gear with varying working depth from the toe to the heel is proposed. The mathematical model of this novel type beveloid gear can be acquired by treating $a = (1.0 + k u)/P_n$ in the proposed mathematical model. Herein, the varying rate of tooth working depth is determined by k , which is a

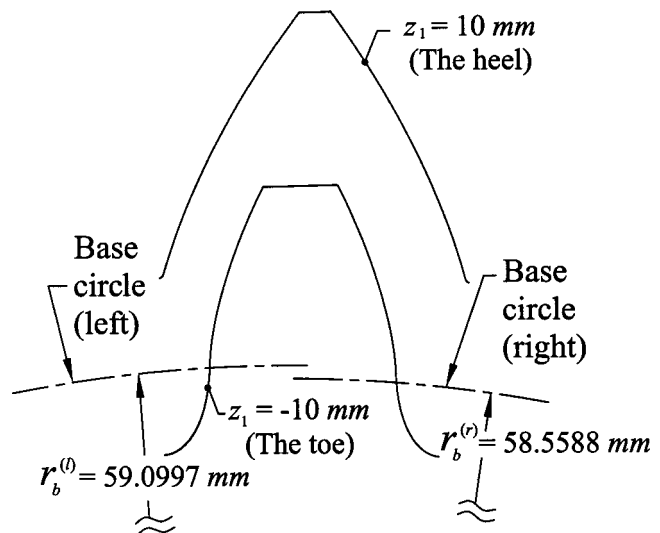


Fig. 9 The tooth profile of helical beveloid gear ($\alpha_n^{(l)} = 20$ deg, $\alpha_n^{(r)} = 30$ deg) and base circles on the plane of rotation

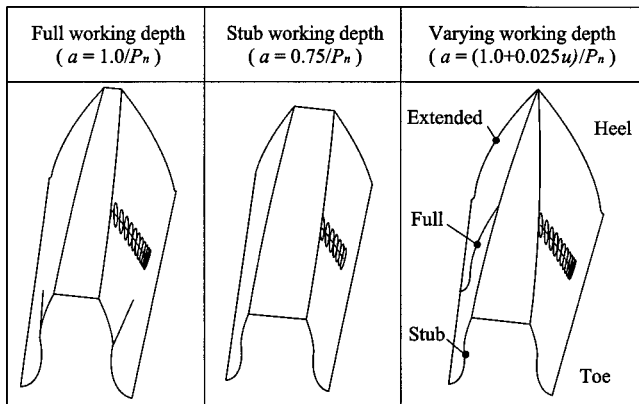


Fig. 10 Straight beveloid gear teeth with full, stub varying working depths

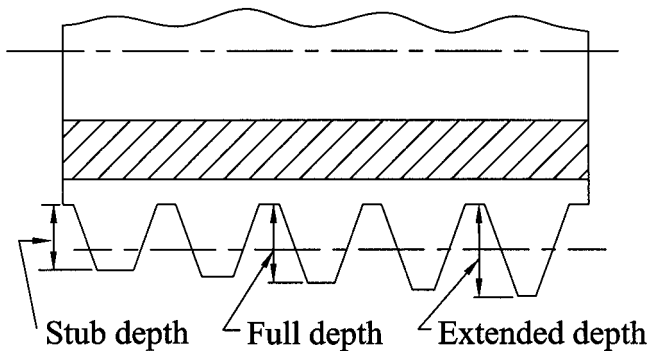


Fig. 11 Schematic of varying depth hob cutter

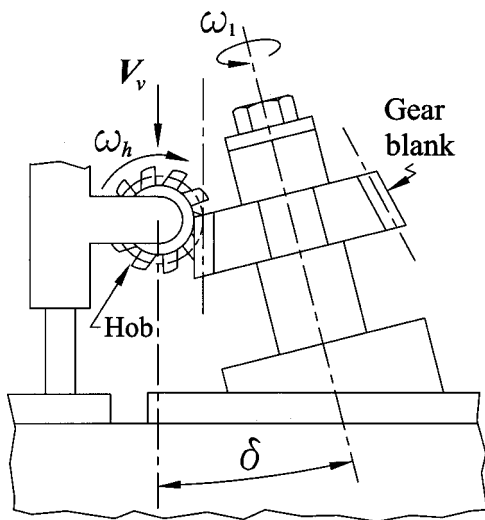


Fig. 12 Schematic of inclining work-arbor taper hobbing

constant in unit (1/mm). A novel type beveloid gear with stub teeth near the toe, full teeth in the central region and extended teeth near the heel can be obtained by choosing an appropriate value of k . Comparisons of the straight beveloid gear teeth with full, stub and varying working depths are illustrated in Fig. 10. The bearing contacts are also plotted on the tooth surfaces. This novel type straight beveloid gear has stub teeth near the toe to prevent undercutting, and full teeth in the central region of tooth width to ensure the contact ratio. Though the extended tooth near the heel may become a pointed tooth, the application of beveloid gears does not become disfigured. Notably, the idea of varying

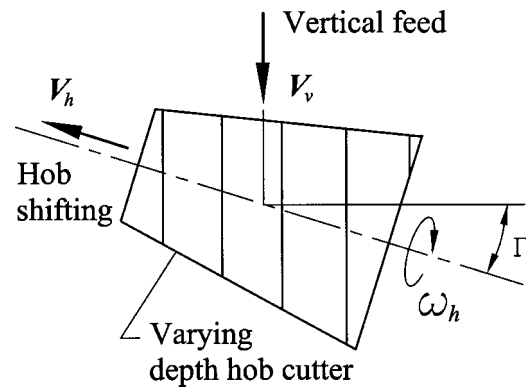


Fig. 13 The movement of hob cutter

working depth comes from the limitation of base circle. Therefore, this method is originally developed for the straight beveloid gear, whose base radii are the same for both sides of the tooth surfaces. However, by choosing proper asymmetrical normal pressure angles to let $r_b^{(l)} = r_b^{(r)}$, this method is also applicable to the undercutting prevention of helical beveloid gears.

To cut this novel type beveloid gear, a novel type hob cutter with varying cutting depths was designed as illustrated in Fig. 11. The cutting depths of the hob cutter linearly increase from one end to the other. Figure 12 schematically depicts the inclining work-arbor taper hobbing [7] for the beveloid gear manufacture. The cutting cone angle δ is given by inclining the work-arbor with respect to the feeding direction of the hob axis. As shown in Fig. 13, by shifting the hob along its rotational axis during the taper hobbing process, the novel beveloid gear with varying working depth can be generated. Despite of rotating with angular velocity ω_h , the hob moves simultaneously in vertical and hob shifting directions with velocities V_v and V_h , respectively. Herein, the setting angle of the hob cutter is Γ . The relation between the gear blank and the axes of hobbing machines can be written as follows:

$$\omega_1 = \frac{N_h}{N_1} \omega_h + \frac{2\pi}{L_1} V_v + \frac{\cos \Gamma}{r_1} V_h, \quad (32)$$

where ω_1 is the angular velocity of the gear blank; N_h is the number of start of the hob cutter (i.e. number of the hob cutter teeth); N_1 is the number of the generated gear teeth, and L_1 is the lead of the generated gear. Equation (32) shows the gear blank rotation in terms of three independent variables ω_h , V_v and V_h . By controlling these variables, the beveloid gear with varying working depth can be generated by CNC hobbing machines.

6 Conclusion

According to the developed mathematical model of beveloid gears, conditions of tooth undercutting have been derived. Some specific phenomena of undercutting on the beveloid gear tooth surface were investigated. To prevent tooth undercutting of beveloid gears, two practicable methods were also proposed. The results of this study help designers and manufactures to design and choose the proper parameters for manufacturing the beveloid gears without tooth undercutting.

Acknowledgment

The authors are grateful to the National Science Council of the R.O.C. for the grant. Part of this work was performed under contract No. NSC 89-2212-E-009-084.

References

- [1] Merrit, H. E., 1954, "Conical Involute Gears," *Gears*, 3rd. ed., Issac Pitman and Sons, London, pp. 165–170.
- [2] Beam, A. S., 1954, "Beveloid Gearing," *Mach. Des.*, **26**, No. 12, pp. 220–238.

- [3] Mitome, K., 1981a, "Table Sliding Taper Hobbing of Conical Gear Using Cylindrical Hob, Part 1: Theoretical Analysis of Table Sliding Taper Hobbing," *ASME J. Eng. Ind.*, **103**, pp. 446–451.
- [4] Mitome, K., 1981b, "Table Sliding Taper Hobbing of Conical Gear Using Cylindrical Hob, Part 2: Hobbing of Conical Involute Gear," *ASME J. Eng. Ind.*, **103**, pp. 452–455.
- [5] Mitome, K., 1983, "Conical Involute Gear, Part1: Design and Production System," *Bull. JSME*, **26**, No. 212, pp. 299–305.
- [6] Mitome, K., 1985, "Conical Involute Gear, Part 3: Tooth Action of a Pair of Gears," *Bull. JSME*, **28**, No. 245, pp. 2757–2764.
- [7] Mitome, K., 1986, "Inclining Work-Arbor Taper Hobbing of Conical Gear Using Cylindrical Hob," *ASME J. Mech. Des.*, **108**, pp. 135–141.
- [8] Mitome, K., 1991, "Conical Involute Gear (Design of Nonintersecting-Nonparallel-Axis Conical Involute Gear)," *JSME Int. J., Ser. III*, **34**, No. 2, pp. 265–270.
- [9] Mitome, K., 1993, "Infeed Grinding of Straight Conical Involute Gear," *JSME Int. J., Ser. C*, **36**, No. 4, pp. 537–542.
- [10] Mitome, K., 1995, "Design of Miter Conical Involute Gears Based on Tooth Bearing," *JSME Int. J., Ser C*, **38**, No. 2, pp. 307–311.
- [11] Mitome, K., Gotou, T., and Ueda, T., 1998, "Tooth surface measurement of conical involute gears by CNC gear-measuring machine," *ASME J. Mech. Des.*, **120**, pp. 358–363.
- [12] Litvin, F. L., 1989, *Theory of Gearing*, NASA Publication RP-1212, Washington D.C.
- [13] Litvin, F. L., 1994, *Gear Geometry and Applied Theory*, Prentice Hall, New Jersey.